



**ARTICLE**

## Effect of Chlorine Salt on Durability of Mineral Admixture Concrete under Different Conditions

Xupeng Chen<sup>1,\*</sup>, Zhuowen Sun<sup>2</sup> and Jianyong Pang<sup>1</sup>

<sup>1</sup>School of Civil Engineering and Architecture, Anhui University of Science and Engineering, Huainan, 232001, China

<sup>2</sup>School of Transportation and Civil Engineering, Nantong University, Nantong, 226019, China

\*Corresponding Author: Xupeng Chen. Email: 1933310001@stmail.ntu.edu.cn

Received: 23 September 2021 Accepted: 12 November 2021

### ABSTRACT

Mineral admixture concrete is a renewable material. It requires less cement than ordinary concrete and is thus beneficial for economical use of resources and environmental protection. To examine the impact of chloride salt on the durability of mineral admixture concrete under various conditions, in this study, test blocks are divided into two major groups: in one group, the test block is eroded by chloride salt on the interior and by sulphate/magnesium salts on the exterior, and in the second group, the test block is eroded by external chloride/sulphate/magnesium salts. Clean water is considered the control group. Dry-wet alternation tests are carried out to investigate the mechanical properties, mass, macromorphology, and ion content of the concrete. Furthermore, a series of methods, such as XRD, FT-IR, SEM, and EDS, are adopted to examine the phase composition and micromorphology of the concrete. The results show that, for the concrete subjected to the corrosion of internal chloride salt and external sulphate/magnesium salts (0–20 cycles), its mechanical properties improve slowly at the initial stage, but at the final stage (80–120 cycles), it is subjected to more severe corrosion compared to those only eroded by a single corrosive ion, such as the chloride/sulfate/magnesium salts. For concretes subjected to external corrosion of chloride/sulphate/magnesium salts, the concrete durability enhances with the concentration increase of the chloride salt.  $Mg^{2+}$  and  $SO_4^{2-}$  could jointly result in destructive damage to the admixture concrete, main generating corrosion products of ettringite, gypsum,  $Mg(OH)_2$ , thaumasite, and M-S-H.

### KEYWORDS

External corrosion; internal corrosion; corrosive ions; dry-wet alternation; durability

## 1 Introduction

With rapid economic development, new large-scale infrastructures, such as cross-sea bridges, undersea tunnels, and dams, have been emerging. Concrete is the main material for infrastructure construction; therefore, its durability is a key factor that determines the service life of these great infrastructures. External corrosive ions in the environment are the main factors that reduce concrete durability [1–3]. In coastal areas and cities with salt lakes in China, there are a variety of ions in local soils and underground water, such as  $CO_3^{2-}$ ,  $K^+$ ,  $Na^+$ ,  $SO_4^{2-}$ ,  $Mg^{2+}$ ,  $OH^-$ , and  $Cl^-$  [4,5]. Among these,  $SO_4^{2-}$ ,  $Cl^-$ , and  $Mg^{2+}$  have the most considerable effect on concrete performance [6,7].  $SO_4^{2-}$  increases the contents of ettringite and gypsum, resulting in volume expansion [8] and mirabilite crystal precipitation [9];  $Mg^{2+}$



promotes the generation of non-cementitious M-S-H inside concrete, weakening concrete properties [10]. Moreover,  $Mg^{2+}$  reacts with the oxyhydril inside the concrete and produces sediments that are difficult to dissolve, such as magnesium hydroxide [11]. Chloride salts differ from other ions because they mainly erode the rebars inside concrete [12]. They are found in seawater, underground water, and salt lake areas and can penetrate mixed concrete during the concrete preparation process, resulting in interior corrosion of the concrete [13,14]. The chemical corrosion caused by corrosive ions in concrete is usually accompanied by effects of various ions [15,16]. The resulting joint damage by the chloride and sulphate salts has been extensively studied. Typically,  $Cl^-$  ion, due to its fast diffusion speed, can inhibit  $SO_4^{2-}$  [17,18]. However, some studies have also reported that  $Cl^-$  promotes the diffusion of  $SO_4^{2-}$  [19].

Most of the corrosive damage that appears in actual environment results from physical and chemical factors jointly instead of only chemical damage. For example, salt lakes and saline areas in Western China are extremely dry with huge water evaporation. In contrast, the coastal areas of China feature alternated flood and ebb tides, which lead to both physical damage caused by dry-wet alternation as well as chemical corrosion caused by corrosive ions. The long-term impacts of dry-wet alternation and salt corrosion increase concrete porosity [20], accelerate the penetration of corrosion ions [21], and worsen the expansion of salt crystals [22].

Therefore, many researchers have tried to enhance concrete durability by reducing the water-binder ratio of concrete, increasing the cement amount [23], applying air-entraining agents, or adopting surface coating approaches [24]. Though these methods have helped improve concrete durability, they are expensive and difficult to implement in construction. Replacing cement by a mineral admixture in concrete is cost and energy effective and environmentally friendly. Therefore, it has become a popular research topic recently. Metakaolin, which is produced by burning kaolin, is found in huge reserves around the world. The fly ash and slag in traditional mineral admixtures have adverse effects on the mechanical performance of concrete at early stages [25]. However, because of its high pozzolanic activity, metakaolin can promote cement hydration, considerably improving the mechanical performance of concrete at the early stage [26]. Ultra-fine fly ash (UFA) is obtained by processing waste from coal-fired power plants. Its activity can be induced and activated during later stages of concrete curing, resulting in secondary hydration and improving the mechanical performance of test blocks [27]. These two active admixtures have particle sizes different from that of cement; thus, adding them to concrete can help achieve high gradation, which not only improves the compactness of the test blocks but also enhances the mechanical performance of concrete at both early and later stages. This solves the problem of adverse effect due to the addition of ordinary mineral admixtures on concrete performance. Therefore, as renewable resources, metakaolin and UFA can be used to replace a part of cement for making concrete. This can not only save resources and protect the environment but also improve concrete performance to some certain extent.

Dhole et al. [28] believed that adding silica fume and fly ash can improve concrete properties for resisting sulphate salt attacks under certain water-binder ratio conditions. Alcamand et al. [29] showed that high-calcium mineral admixtures can more likely generate gypsum and ettringite, resulting in unsatisfactory concrete properties for resisting sulphate attacks. Goncalves et al. [30] believed that  $Mg^{2+}$  considerably impacts metakaolin (MK) concrete, but Mardanic et al. [31] expressed contrasting views, reporting that MK can significantly reduce concrete expansion in a magnesium sulphate solution, thereby enhancing concrete property of resisting  $Mg^{2+}$  corrosion.

Most existing studies about the ion-resisting properties of mineral admixture concrete are conducted based on a specific type of ion. For synergic corrosion caused by a variety of ions, different researchers still hold contradictory opinions. Moreover, such synergic corrosion is usually caused by ions outside concrete. In many projects situated in areas with high salinity and in coastal areas, concrete is usually prepared using local underground water or lake water [14,32]. Compared with water used in laboratories,

such types of water contain certain amounts of chloride salts that can result in internal corrosion of concrete. Therefore, in this study, we compare the differences between internal corrosion caused by chloride salts and external corrosion caused by sulphate/magnesium salts, and external corrosion caused by chloride/magnesium/sulphate salts; furthermore, we study the impact of chloride salt concentration on concrete durability by adopting the dry-wet alternation method, examining the physical properties and sulphate ion concentration periodically. X-ray diffraction (XRD), Fourier-transform infrared spectroscopy (FTIR), and scanning electron microscopy (SEM) are used to analyse the physical composition and micromorphology of concrete, thus exploring the deterioration mechanism of mineral admixture concrete under different corrosive conditions.

## 2 Experimental Procedures

### 2.1 Experimental Materials and Preparation

The materials we adopt in this study include PO42.5 Portland cement produced in Bagongshan of Huainan City, white metakaolin, with approximately 1.8  $\mu\text{m}$  average particle size, produced by Shanghai Lingdong Company (China), and UFA, with approximately 5.95  $\mu\text{m}$  average particle size, produced by Henan Zhengzhou Huifeng New Materials Co., Ltd., China. The chemical compositions of the cement and mineral admixtures are given in Table 1, and the particle size distribution of metakaolin and UFA are given in Fig. 1. We adopt 5–15 mm continuously graded gravels and medium sands with approximately 2.9 fineness modulus, obtained from Huaihe River, and polycarboxylate-based superplasticiser produced by Shaanxi Qinfen Construction Materials Co., Ltd., China. As the water reducer, which exhibits approximately 37% water reduction rate and 40% solid content. Its physical properties are given in Table 2.

**Table 1:** Chemical composition of cementing materials in the test (%)

Composition	SiO <sub>2</sub>	Al <sub>2</sub> O <sub>3</sub>	CaO	Fe <sub>2</sub> O <sub>3</sub>	K <sub>2</sub> O	SO <sub>3</sub>	P <sub>2</sub> O <sub>5</sub>	Na <sub>2</sub> O	MgO
MK	56.28	42.01	0.03	0.59	0.12	0.22	0.09	0.13	0.16
UFA	54.12	35.22	2.27	5.33	0.42	0.53	0.17	0.29	0.61
Cement	21.91	3.11	68.82	2.71	0.51	1.05	0.28	0.03	0.71

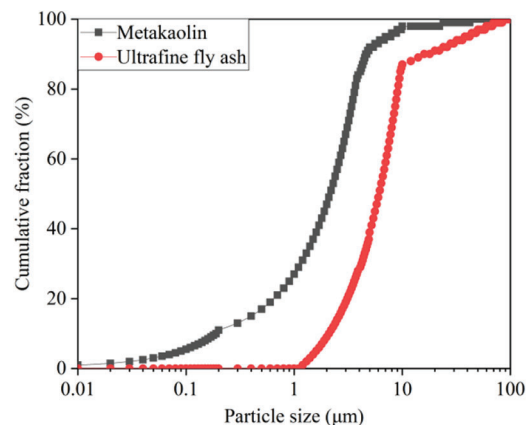


**Figure 1:** Particle size distribution of mineral admixtures

**Table 2:** Physical properties of materials

Physical properties	Aggregate		Cementitious materials		
	Rubble	Sand	Cement	Metakaolin	Ultra-fine fly ash
Density (g/cm <sup>3</sup> )	/	/	3.14	0.6	2.1
Specific surface area (m <sup>2</sup> /kg)	/	/	350	3500	624
Bulk density (kg/m <sup>3</sup> )	1534	1577	/	/	/
Apparent density (kg/m <sup>3</sup> )	2630	2621	/	/	/

The test is composed of two major groups. According to literature [14,32], lots of cast-in-place concrete structures in saline and coastal areas are prepared using underground water and river water. This results in internal salt corrosion in the concrete. We set the first major group (Major Group 1) to study the synergic concrete deterioration resulting from internal chloride and external compound (sulphate/magnesium) salts. According to the chemical composition of ions in soil and underground water in the offshore and western regions of China, and on the basis of relative specifications (GB/T50082–2009) [33], we take 5% MgSO<sub>4</sub> solution as the external corrosive solution and 0.5% and 3.5% NaCl solutions as the internal corrosive solutions, which are referred to as C0.5 + M and C3.5 + M, respectively. The second major group (Major Group 2) is only eroded by external chloride/sulphate/magnesium salts. Its external corrosive media are 5% MgSO<sub>4</sub> solution, 5% MgSO<sub>4</sub>+0.5% NaCl solution, and 5% MgSO<sub>4</sub>+3.5 NaCl solution, which are referred to as C0 M, C0.5 M, and C3.5 M, respectively. We also used clean water as the solution of the control group, Group P. For more details, please see Table 3.

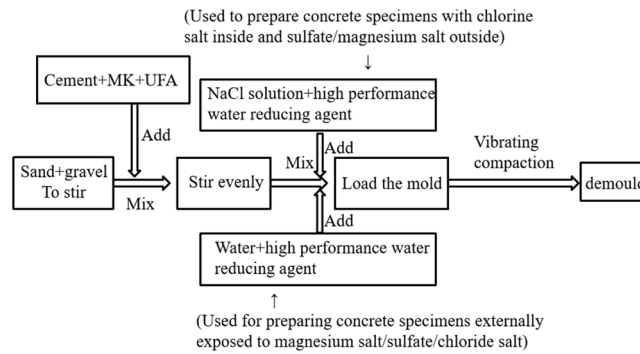
**Table 3:** Test piece number and solution type

Number	Internal corrosion	External corrosion		28 days compressive strength (MPa)
	NaCl	NaCl	MgSO <sub>4</sub>	
P	0	0	0	58.8
C0.5 + M	0.5%	0	5%	54.3
C3.5 + M	3.5%	0	5%	50.1
C0 M	0	0	5%	59.2
C0.5 M	0	0.5%	5%	57.5
C3.5 M	0	3.5%	5%	58.1

Table 4 shows the mix ratio design of the admixture concrete. Steps to prepare concrete include: put the sands and gravels into mixer to mix for over 1 min; then, put cement, metakaolin, and UFA in and mix for at least 2 mins till the cementing material and the aggregates are well mixed evenly; finally, mix the water reducer with the well-prepared NaCl solution (Major Group 1), or mix the water with the water reducer (Major Group 2), and put the mixture into the mixer. After the mixing is finished, put the mixture into mould and then move the mould to the vibration table to have it vibrated and compacted (Fig. 2). Then, put the mould aside and wait for 24 h. Thereafter, demould and put the concrete blocks in a standard curing room at (20 ± 2)°C and ≥ 95% humidity for 28 days.

**Table 4:** Mix ratio design of mineral admixture concrete (kg/m<sup>3</sup>)

Component	Cement	MK	UFA	Sand	Aggregate	Water	Water reducing agent
Parameter	350	50	100	619	1101	180	4

**Figure 2:** Process of making concrete test block

## 2.2 Test Method

We adopted the dry-wet alternation method. The operation process is: soak the test blocks for 15 h → dry them at room temperature for 1 h → dry in dryer at 60°C for 7 h → cool for 1 h. The whole process is a 24 h cycle. At 20, 40, 80, and 120 cycles, we tested the compressive strength, mass, and sulphate ion content as well as the micro properties of the test blocks. To ensure concentration stability of all solutions, we replaced the solutions with new ones every 10 days.

### 2.2.1 Testing Physical Properties

The concrete blocks made for the test were non-standard blocks sized 100 mm × 100 mm × 100 mm. The test operation was designed based on provisions of (GB/T50081—2002) [34]. Since the test blocks adopted in this study were not standard, we multiplied the conversion coefficient of 0.95 and calculated the rate-of-change of the compressive strength using formula (1).

The mass was measured by the balance (accurate to 0.01 g). The rate-of-change of the mass was calculated using formula (2).

$$\Delta F = \frac{F_N - F_0}{F_0} \times 100\% \quad (1)$$

where  $\Delta F$  is the rate-of-change of compressive strength;  $F_N$  is the compressive strength of the samples after N times of dry-wet alternations;  $F_0$  is the compressive strength of concrete that has not been eroded.

$$\Delta M = \frac{M_N - M_0}{M_0} \times 100\% \quad (2)$$

where  $\Delta M$  is the rate-of-change of the concrete mass;  $M_N$  is the concrete mass after N cycles of dry-wet alternations;  $M_0$  is the concrete mass that has not been eroded.

### 2.2.2 Testing Sulphate Ion Content

The barium sulphate precipitation method was used to test the sulphate ion content. In this study, we adopted the impact drill to collect powder from the concrete test blocks. We drilled the blocks

downwards to 4 mm, 8 mm, 12 mm, 16 mm, and 20 mm depths to collect powders. For each test block, we collected 5 powder samples. After weighing, the samples were put into dryer and then soaked in diluted water for 48 h till the  $\text{SO}_4^{2-}$  in the concrete was completely dissolved. After that, we filtered it using filter paper, added  $\text{BaCl}_2$  solution, and adopted the barium sulphate precipitation method to measure the sulphate ion content in each sample. The test operation was designed based on relative provisions in GB/T176–2008 [35] and SL352–2006 *Test Code for Hydraulic Concrete*. The sulphate ion content was calculated using formula (3).

$$C\% = \frac{c \times (M_3 - M_2)}{M \times M_1} \times 100\% \quad (3)$$

where  $C\%$  is the mass proportion of the sulphate ion;  $c$  is mole mass of the testing ions;  $M$  is the mole mass of the barium sulphate;  $M_1$  is the mass of the concrete powder for soaking;  $M_2$  is the mass of the crucible; and  $M_3$  is the total mass of the barium sulphate and the crucible.

### 2.2.3 Analysis of Physical Compositions

Physical composition analysis was carried out at 40 and 120 cycles. The D/max-2550 XRD instrument was used to perform XRD analysis. For this test, the scanning step was set as  $0.02^\circ$ . The NICOLET IS 50 infrared spectrometer produced by American company was used to conduct the FTIR test on the powder samples. We collected powders at depths in ranges 2–4 mm inwards along the eroded surface of the test block, and sieved using  $75 \mu\text{m}$  sieves to remove aggregates with comparatively large particle sizes.

### 2.2.4 Analysis of Micromorphologies

When 120 d alternation was reached, micromorphology analysis was conducted on all test blocks. We adopted cold field SEM and energy dispersive spectrometry (EDS) to observe and analyse the micromorphologies. Samples for this test were acquired from the test blocks subjected to the compressive strength tests. Mortar slices with 2–4 mm thickness were taken from the test block surface and placed in absolute alcohol to end their hydration. Then, the samples were placed in a dryer at  $60 \pm 5^\circ\text{C}$  and dried till constant mass was reached. After that, the test blocks were subjected to grinding and polishing treatment, and placed under vacuum and conductive coating to improve the conductivity before the final SEM test.

## 3 Results

### 3.1 Analysis of Macro Physical Properties

Fig. 3 shows the rate-of-change of the mechanical property as well as the mass of the concrete samples in various solutions. The broken line represents joint corrosion by the internal chloride salt and the external magnesium/sulphate salts. The solid line indicates that the admixture concrete is only corroded by the external sulphate/magnesium salts or sulphate/magnesium/chloride salts.

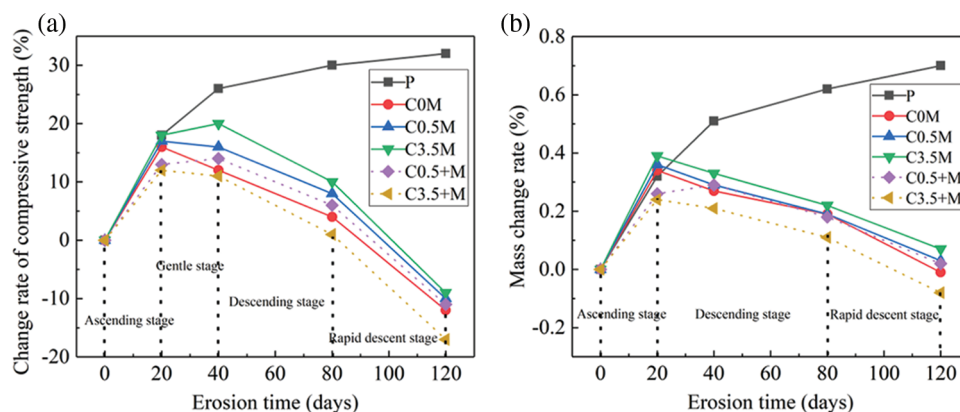


**Figure 3:** Changes in physical properties: (a) Change rate of compressive strength, (b) Mass change rate

Except Group P, for the mineral admixture concrete in other 5 solutions, the changing law of compressive strength is as below: rising stage → gentle stage → declining stage → rapid declining stage. During 0–20 dry-wet alternation cycles, the concrete is getting hydrated. Because of the secondary hydration caused by metakaolin and UFA, concrete mechanical properties keep improving. Group C0.5 + M and Group C3.5 + M show only 13% and 11% improvement rates, which are both lower than those of other groups. The reason for this is that the internal chloride salt corrosion would inhibit  $C_3A$  and  $SO_4^{2-}$  from generating ettringite and promote the transformation of AFm towards Friedel salts [36]. AFt and AFm are two hydration products that are generated not so much at the initial stage. The two play the role of filling up pores, compensating shrinkage, and accelerating the process of hydration. The internal corrosion of chloride salt indirectly slows down the strength improvement of C0.5 + M and C3.5 + M. When the corrosion reaches 40 days, the increase rate of the compressive strength of Group C0.5 + M rises, reaching 14%. The same data of the remaining groups show a declining trend because although the small amount of  $Cl^-$  inside the concrete can slightly slow down the hydration process, it can also inhibit  $SO_4^{2-}$  corrosion, thereby reducing amount of  $SO_4^{2-}$  and  $Mg^{2+}$  that entered the substrate. In this way, only some ettringite was generated to fill the pores. When the dry-wet alternation reached 120 days, with the increase of chloride salt concentration, the declining rate of the compressive strength was accelerated: the compressive strength of Group C0.5 + M concrete declined by 12%, while that of Group C3.5 + M declined by 17%. The higher the chloride ion concentration inside is, the slower the hydration process of the mineral admixture concrete is, and the weaker the compactness is. Therefore, the performance in resisting sulphate salt corrosion was greatly weakened.

It can be seen from the mass changes of the mineral admixture concrete that except for the concrete test blocks of Group P, the mass changes of the remaining groups indicate three stages: rising stage → declining stage → rapid declining stage. During 0–20 days of cycle, the mass of the mineral admixture concrete keeps increasing because of two reasons: one is the continuous hydration of the unhydrated cement and the secondary hydration of the mineral admixture, and the other is the generation of a small amount of corrosion products, such as ettringite, magnesium hydroxide, and Friedel salts [37]. After reaching 120 d dry-wet alternations, the growth rates of masses of the five different test blocks (C0.5 + M, C3.5 + M, C0 M, C0.5 M, and C3.5 M) reached 0.02%, -0.08%, -0.01%, 0.03%, and 0.07%, respectively. Compared with the groups of test blocks where the concrete was corroded by external chloride/sulphate/magnesium salts, the concentration of chloride ions was directly proportional to the mass growth rate; with the increase of  $Cl^-$  concentration, the mass growth rate gradually increases; chloride ions can inhibit the generation of ettringite, thereby slowing down the destruction rate of concrete. In addition, it was found that the mass increase rate of Group C0.5 + M was higher than that of the C0 M group; according to Fig. 1a, at 120 cycles, the growth rate of the compressive strength of Group C0 M reaches -12% and that of Group C0.5 + M reaches -11%, which can further indicate that the incorporation of a small amount of  $Cl^-$  can delay the destruction of sulphate salt.

Comprehensive comparison shows that when the concrete is corroded from the interior by interior chloride salt and from the exterior by the sulphate and magnesium salts, the compressive strength reduction and the mass loss are both higher than those of concrete corroded by a single external compound salt; under low concentration condition of internal chloride salt, such as Group C0.5 + M, the loss rate of physical property was lower than that of C0M, and so, the loss rate of the physical property is  $P < C3.5 M < C0.5 M < C0.5 + M < C0 M < C3.5 + M$ .

### 3.2 Macromorphology Analysis

Fig. 4 shows the macromorphology of the mineral admixture concretes that have experienced 120 days of alternations. The surfaces of the test blocks in Group P, except for a small amount of air bubbles on the surface, are relatively flat and smooth with good integrity; the three cementing materials, including the

metakaolin, UFA, and cement, have different particle sizes and can fill up pores. So, adding these materials helps achieve excellent gradation inside the concrete; therefore, the mineral admixture concrete is endowed with high macro-compactness.

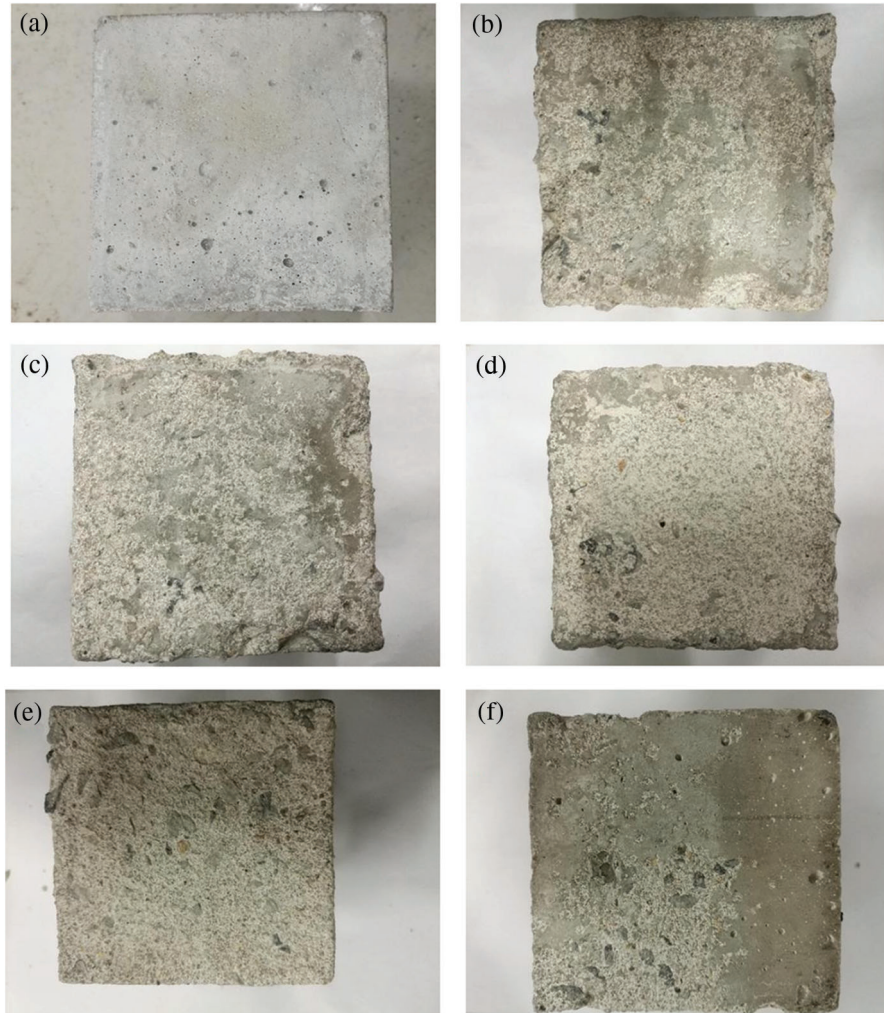


**Figure 4:** Macromorphology of concrete test blocks in each group after 120 dry-wet cycles (a) P, (b) C0.5 + M, (c) C3.5 + M, (d) C0 M, (e) C0.5 M, (f) C3.5 M

Figs. 4b–4f show the macromorphology of the mineral admixture concretes eroded by  $\text{MgSO}_4$  and  $\text{NaCl}$  solutions. The cement mortar structures of the 5 groups of test blocks are severely damaged, and the surface of the mineral admixture concrete presents a powdery state, mainly due to the generation of M-S-H. M-S-H is a corrosion product with no cementing ability, and its existence will cause softness and peeling of orthopaedics. There are two ways to generate M-S-H; one is ion replacement: the ionic radius of  $\text{Mg}^{2+}$  is approximately 72 pm while the radius of  $\text{Ca}^{2+}$  is 99 pm; thus, the ionic radii of the two are similar [38]. C-S-H can be easily decalcified to form M-S-H. The other is chemical reaction:  $\text{Mg}^{2+}$ ,  $\text{SiO}_2$ , and hydroxyl can react to generate M-S-H; because UFA and metakaolin contain more active  $\text{SiO}_2$ , it can greatly promote the generation of M-S-H.

Fig. 4b shows the macromorphology of Group C0.5 + M. A large part of mortar aggregates on the test block surface peel off; with the increase of internal chloride salt concentration, the peeling-off area of the aggregate is further increased, as shown in Fig. 4c; the corners of the test blocks begin to fall off, indicating severe damage. If the test block is only eroded by the external  $\text{MgSO}_4$  solution, as shown in Fig. 4d, the aggregate peeling-off area on the surface of the test block is larger than that of Group C0.5 + M, and the upper right corner of the concrete is damaged; when the external corrosion is caused by the  $\text{MgSO}_4 + \text{NaCl}$  solution (Fig. 4e), the corrosion damage is slowed down; with increasing NaCl solution concentration, the corrosion of sulphate and magnesium salts is inhibited, as shown in Fig. 4f, and the area of aggregate peeling-off on the surface of the test block is significantly reduced.

### 3.3 Analysis of $\text{SO}_4^{2-}$ Content

Fig. 5 shows the sulphate ion content of the mineral admixture concrete when the five different corrosive compound solutions erode the mineral admixture concrete; when sulphate ions diffuse, the sulphate ions of the corrosion solution accumulate on the surface of the test blocks under the action of the ion concentration gradient; then, the ions diffuse into the interior; as the diffusion depth increases, the concentration gradient of ions decreases rapidly, and the saturation of pores reduces greatly, which increases the diffusion resistance of ions. Therefore, as the depth increases, the concentration of sulphate ions reduces greatly.

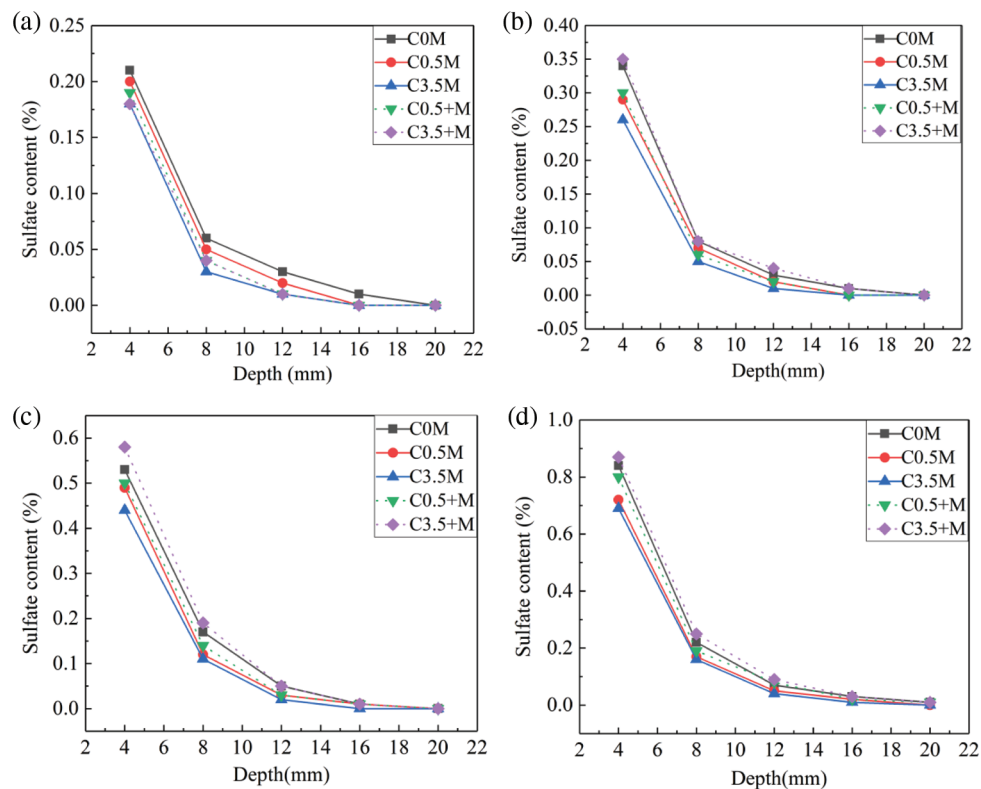


**Figure 5:** Sulphate ion content of concrete in different corrosion cycles: (a) 20 days, (b) 40 days, (c) 80 days, (d) 120 days

When reaching 20 cycles of dry-wet alternations, the maximum sulphate ion content of C0.5 M group is 0.2%, and the same data of C0.5 + M is 0.19%; when the chloride ion content increases to 3.5%, the maximum sulphate ion content of Group C3.5 + M and Group C3.5 M both reach 0.18%. This is lower

than that of Group C0 M, which is not corroded by chloride ions. Calcium aluminate hydrate (CAH) and the calcium sulphoaluminate hydrate (AFm), which are the secondary hydration products of UFA and metakaolin, can combine with the chloride salts to produce Friedel salts [39], thereby reducing the internal pores of the mineral admixture concrete. In this case, the above two secondary hydration products can inhibit the corrosion of sulphate ions to some extent. Therefore, for both external and internal corrosion of ions, with increasing chloride ion content, the sulphate ion content gradually decreases.

When reaching 40 cycles of dry-wet alternations, the maximum sulphate ion content of Group C3.5 + M reaches 0.35%, which is higher than the maximum ion content of Group C0 M (0.34%). Group C3.5 + M is subjected to the corrosion of the highly concentrated chloride ions inside the test blocks at the early curing stage. This leads to slow hydration and low compactness. As the corrosion time increases, the role of chloride ions in hindering corrosive ions becomes limited; the mineral admixture concrete will have cracks and pores under the continuous corrosion of corrosive ions, so the concentration of sulphate ions increases accordingly; as for Group C0.5 + M, the small number of chloride ions has little effect on the early hydration of concrete, so the content of sulphate ions is 0.27%. For the C0.5 M and C3.5 M groups, the admixture concretes are corroded by the external chloride salts and the magnesium sulphate salts; the  $Mg^{2+}$  and  $SO_4^{2-}$  in the solution will react with the  $Ca(OH)_2$  on the surface of the mineral admixture concrete, and generate the magnesium hydroxide layer and the gypsum layer [40]; the external sulphate ions entering the concrete are inhibited to a certain extent, the maximum sulphate ion content is 0.29% in Group C0.5 M, and is 0.26% in Group C3.5 M.

With increasing alternation cycle, the maximum sulphate ion contents of Group C0.5 + M and Group C3.5 + M, which are subjected to the corrosion of the interior chloride salts, gradually exceed the contents in Group C0.5 M and Group C3.5 M corroded by the external compound salts. When reaching 120 cycles of alternations, the maximum sulphate ion contents of Group C0.5 M and Group C3.5 M are 0.72% and 0.69% respectively, and the same data of Group C0.5 + M and Group C3.5 + M reach 0.80% and 0.87%; compared with 80 cycles, the content of sulphate ions when reaching 120 cycles increase by 50%–60%. Due to the influence of early hydration, the two groups of concrete eroded by internal chloride salts have lower compactness than the other groups. In the later period of corrosion, under the interaction of the corrosion products, such as magnesium hydroxide, M-S-H, gypsum, ettringite, and thaumasite, the mortar on the concrete surface peels off, and the internal corrosion products continue to form and grow. This causes continuous crack generation and expansion and provides a convenient channel for the sulphate ions to diffuse into the concrete. For Group C0 M, Group C0.5 M, and Group C3.5 M, when the external chloride salt concentration increases from 0% to 3.5%, the maximum sulphate ion content decreases from 0.84% to 0.69%. For the three types of concretes that are subjected to external chloride salt corrosion, the Friedel salt content inside the test blocks increased during the corrosion process with increasing content of external chloride salt. At 120 days of corrosion, the pH value inside the concrete decreased, resulting in Friedel hydrolysis. Moreover, during the hydrolysis process of the Friedel salt, a great number of free  $Cl^-$  would be released [41]. For  $SO_4^{2-}$ , since its volume is bigger than  $Cl^-$ , it diffuses slowly and is affected by  $Cl^-$ , which diffuses faster during the  $SO_4^{2-}$  migration process. The higher is the external  $Cl^-$  content, the higher is the Friedel salt content, and the more is free  $Cl^-$  released from Friedel salt hydrolysis. Therefore, at the latter stage, the increase of external chloride salt will slower the diffusion of  $SO_4^{2-}$ .

The ion synergism affects concrete greatly. When the corrosive ions erode the concrete,  $Mg^{2+}$  and  $SO_4^{2-}$ , react with oxhydroxyl, they generate corrosion products such as magnesium hydroxide and gypsum. This reduces the pH value inside the concrete and accelerates the diffusion of  $Mg^{2+}$ . Moreover, the decomposition of Friedel salt generates massive  $Cl^-$ , which enter the concrete. The invasion of  $Mg^{2+}$  accelerates the production of more M-S-H inside the concrete. This worsens the aggregate peeling-off and

the cracking of the test blocks and further accelerates the diffusion of  $\text{SO}_4^{2-}$ , thereby producing more ettringite and gypsum and resulting in secondary expansion damage to the concrete.

### 3.4 Phase Composition Analysis

#### 3.4.1 X-Ray Diffraction Analysis

To reveal the corrosion time clearly, Group P was taken as the control group in this study to figure out the changes of the chloride salt concentration, and the effects of the interior and exterior chloride salt corrosion on the phase composition inside the mineral admixture concrete. Group P, Group C0.5 + M, and Group C3.5 + M were taken to form a big group to study the interior chloride salt corrosion, while Group C0 M, Group C0.5 M, and Group C3.5 M were used to form another big group to study the exterior chloride salt corrosion.

Fig. 6 shows the XRD spectra of each group of mineral admixture concretes when reaching 40 cycles of corrosion. The phase composition of each group of test blocks mainly includes quartz, calcite, ettringite, calcium hydroxide, ettringite, magnesium hydroxide, and gypsum. The quartz and the calcite possess the most significant diffraction peaks, which both come from the aggregate of concrete. As shown in Fig. 6a, the control Group P is not corroded by ions in the clear aqueous solution. The pozzolanic effect of the two mineral admixtures of metakaolin and UFA, will also produce a small amount of ettringite. Therefore, Group P has a weak ettringite diffraction peak. With the increase of the internal chloride salt concentration, the diffraction peaks of ettringite, gypsum, and magnesium hydroxide increase, indicating that the increase of the internal chloride salt concentration worsens the concrete damage. As shown in Fig. 6b, if the concrete is corroded by external chloride/magnesium/sulphate salts, the concentration of external chloride salt increases, the diffraction peak of Friedel salt continues to increase, and the ettringite diffraction peak decreases, as the diffusion of  $\text{Cl}^-$  is relatively fast. When ions enter the interior of the concrete,  $\text{Cl}^-$  will react with Al prior to  $\text{SO}_4^{2-}$  and form Friedel salts [42]. This refines the pores, slows down the diffusion rate of  $\text{SO}_4^{2-}$ , and inhibits the generation of ettringite. Similarly, the massive generation of Friedel will also inhibit the generation of magnesium hydroxide; therefore, with the increase of  $\text{Cl}^-$  concentration in the external solution, the content of the corrosion products will decrease. In this case, the concrete loss will also be reduced accordingly.

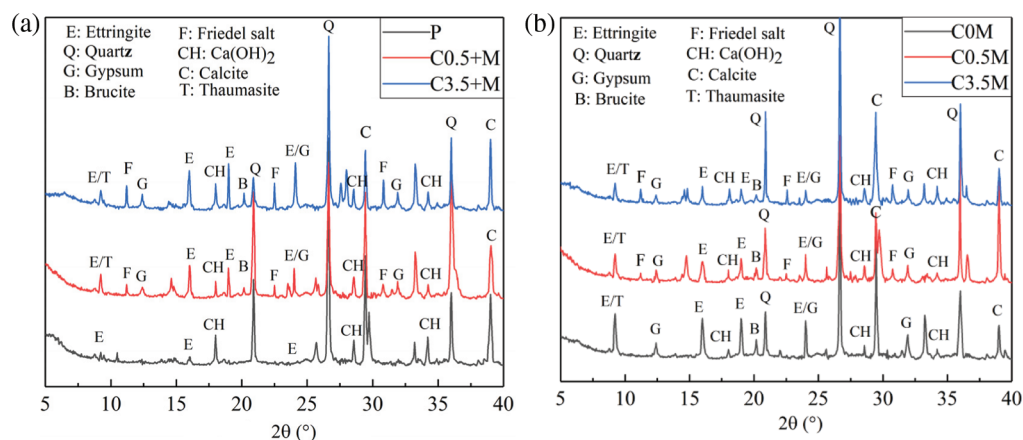


**Figure 6:** Dry-wet cycle for 40 days: (a) internal chlorine salt corrosion, (b) external chlorine salt corrosion

When reaching 120 times of dry-wet alternations, as shown in Fig. 7, the diffraction peaks of  $\text{Ca}(\text{OH})_2$  in Group C0.5 + M, Group C3.5 + M, and Group C0 M disappear, those diffraction peaks of Group P, Group C0.5 M, and Group C3.5 M reduce greatly, and those diffraction peaks of gypsum and magnesium hydroxide increase gradually. This indicates that the  $\text{Ca}(\text{OH})_2$  has been largely consumed, causing the pH value drop

inside the test block [43]. Meanwhile, the  $Mg^{2+}$  flows faster in low-alkali environment [44] and reacts with the hydroxyl faster to produce magnesium hydroxide with very low solubility. Since the ettringite could decompose in low pH environment, and the secondary ettringite cannot be formed, the transformation towards gypsum is thereby accelerated. Therefore, the diffraction peaks of magnesium hydroxide and gypsum gradually increase, while the diffraction peaks of ettringite gradually decrease. For Group C0.5 M, the diffraction peak of the corrosion products is lower than that of Group C0 M. Although the internal chloride salt slows down the corrosion to the physical properties of the concrete at the initial stage, the  $Cl^-$  has always been inhibiting the corrosion of  $SO_4^{2-}$  and  $Mg^{2+}$ , even a small amount of  $Cl^-$  in the concrete could accelerate the hydration rate of the tricalcium silicate [45,46], increase the physical adsorption of corrosive ions, and reduce the formation of corrosion products by chemical bound ions inside the matrix. When the internal chloride salt concentration is 3.5%, the diffraction peaks of corrosion products such as ettringite, magnesium hydroxide, and gypsum are higher than all other groups. In addition, the inhibitory effect of external chloride ions on the corrosion products is much higher than that of the internal chloride ions. As shown in Fig. 7, the diffraction peaks of the corrosion products of Group C0.5 M and Group C3.5 M are lower than those of Group C0.5 + M and Group C3.5 + M. Similar to the law with 40 days' corrosion time, with the increase of the external chloride salt concentration, the diffraction peak of corrosion products decreases.

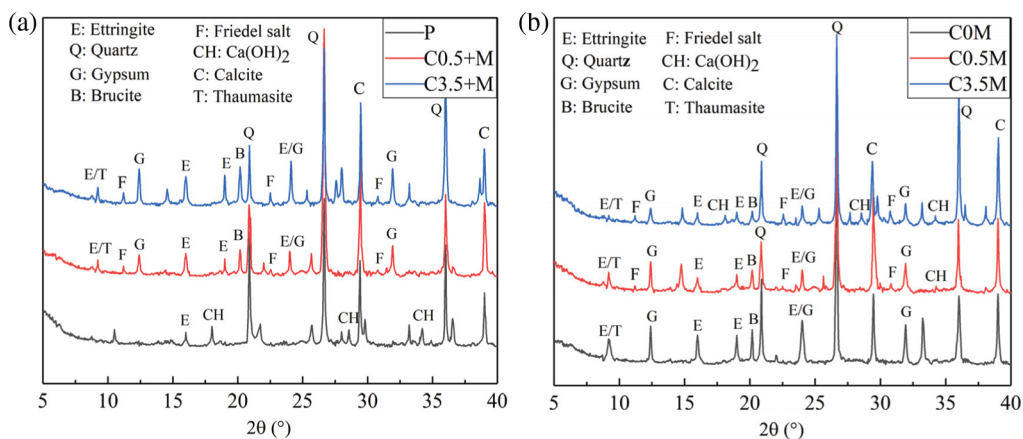


**Figure 7:** Dry-wet cycle for 120 days: (a) internal chlorine salt corrosion, (b) external chlorine salt corrosion

### 3.4.2 Fourier-Infrared Spectroscopy Analysis

Compared with the XRD tests, the FTIR spectra can effectively distinguish and identify thaumasite, M-S-H, and other substances; therefore, FTIR was used to examine the test blocks when reaching 40 and 120 cycles of alternation. The spectrum is as shown in Fig. 8.

When reaching 40 cycles, as shown in Fig. 8a, the intensity and width of the absorption peaks of various groups are different from each other. There are bending vibration peaks and stretching vibration peaks of C-O bond at wavenumber positions of  $872.1\text{ cm}^{-1}$  and  $1410.1\text{ cm}^{-1}$ . These peaks are mainly from the calcite in the aggregate [47]. There is a stretching vibration peak of the S-O bond at  $1165\text{ cm}^{-1}$ , and bending absorption peaks of the Al-O bond at  $845.4\text{ cm}^{-1}$  and  $552.1\text{ cm}^{-1}$ . It can be judged that the ettringite is one of the corrosion products. The characteristic absorption peak of gypsum is located at  $1105.5\text{ cm}^{-1}$ , which is caused by the stretching vibration of the S-O bond [48]. In addition, at  $502.3\text{ cm}^{-1}$  and  $711.1\text{ cm}^{-1}$  in the figure, there are a bending vibration peak and a stretching vibration of the Si-O bond, respectively. This proves the existence of thaumasite [49]. Comparing the peak sizes of ettringite, gypsum and thaumasite in each test block, it can be seen that  $C0\text{ M} > C3.5 + M > C0.5 + M > C0.5\text{ M} > C3.5\text{ M}$ .

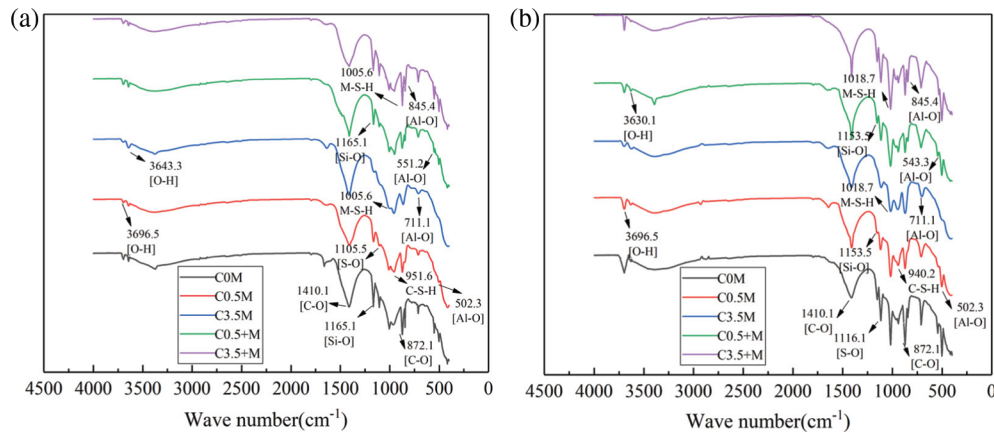


**Figure 8:** FTIR spectra of each group of concrete in different corrosion days: (a) 40 cycles, (b) 120 cycles

When reaching 120 cycles of corrosion, as shown in Fig. 8b, the absorption peak size changes and the wavenumber shifts. For ettringite, the absorption peak intensity of the Si-O bond at  $1165\text{ cm}^{-1}$  and the Al-O bond at  $551.2\text{ cm}^{-1}$  reduce, red shift occurs, and the group tends to be unstable. In contrast, the characteristic absorption peak of gypsum shifts from  $1105\text{ cm}^{-1}$  to  $1116\text{ cm}^{-1}$ , a blue shift occurs, and the absorption peak increases. At this time, the pH value decrease of the test block causes ettringite decomposition. This promotes the generation of gypsum. This is consistent with the results of the XRD analysis. In Fig. 8a, there is a characteristic peak of M-S-H at  $1005.6\text{ cm}^{-1}$  [50]. When the corrosion reaches 120 times, the characteristic absorption peak is greatly enhanced, and blue shift occurs, the group tends to be stable, the asymmetric vibration peak of Si-O-T in the hydration product C-S-H moves from  $951\text{ cm}^{-1}$  to  $940.2\text{ cm}^{-1}$ , and the characteristic absorption peak is weakened. This indicates that the C-S-H is massively decalcified to generate M-S-H. The comparison of the absorption peak size in the figure shows that C3.5 + M reaches the maximum absorption peak here. At this time, the absorption peak sizes of the corrosion products such as ettringite, gypsum, and moissanite are: C3.5 + M > C0 M > C0.5 + M > C0.5 M > C3.5 M. In Fig. 8a, there is a characteristic absorption peak of  $\text{OH}^-$  at  $3640.3\text{ cm}^{-1}$ . It is known that [51] here is the characteristic absorption peak of  $\text{Ca}(\text{OH})_2$ . Since a large amount of  $\text{Ca}(\text{OH})_2$  needs to be consumed during the reaction, corrosion products such as  $\text{Mg}(\text{OH})_2$ , ettringite, and gypsum are generated. Therefore, the characteristic peak of  $\text{Ca}(\text{OH})_2$  is greatly reduced when the corrosion reaches 120 times; at this time, the characteristic peaks of the samples C0 M and C3.5 + M disappear. In addition, there is a characteristic absorption peak of  $\text{Mg}(\text{OH})_2$  at  $3696\text{ cm}^{-1}$  [52]. As the cycle progresses, the characteristic peak of  $\text{Mg}(\text{OH})_2$  of the sample C0 M is the strongest.

### 3.5 Micromorphology Analysis

Fig. 9 shows the micromorphology of the concrete after 120 cycles of corrosion. The micromorphologies of the concretes differ under different corrosion conditions. When the concrete is put in clean water, as shown in Fig. 9a, the unhydrated particles on concrete surface are closely linked with the hydration products; due to the high pozzolanic activity of metakaolin and UFA, the surface of the spherical UFA is almost covered by the hydration products. In general, the concrete is quite compact, indicating good pozzolanic characteristics. Fig. 9b shows the micromorphology of concrete in  $\text{MgSO}_4$  solution. Compared with the samples of Group P, the overall connectivity is poor on the loose and porous concrete surface.

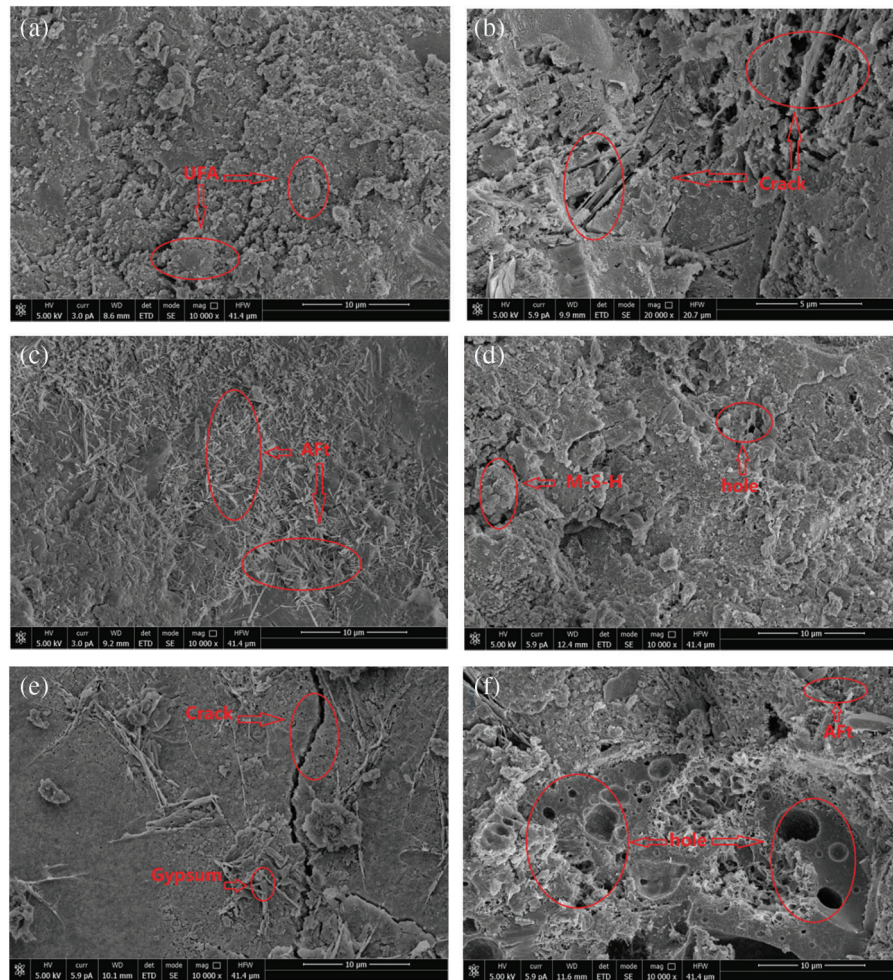


**Figure 9:** Micromorphology of each group of concrete when the cycle time is 120 days: (a) P, (b) C0 M, (c) C0.5 M, (d) C3.5 M, (e) C0.5 + M, (f) C3.5 + M

After exposure in the  $\text{MgSO}_4+\text{NaCl}$  solution, as shown in Fig. 9c, the concrete is covered by a large area of dense and thin needle-like corrosion products. It is determined by conducting the EDS analysis (Fig. 10a) that the main element compositions of these needle-like corrosion products include Ca, O, S, Si, and Al. According to the morphological characteristics [53,54], it can be preliminarily judged that the substance is ettringite. The rapid increase in the content of ettringite leads to the continuous increase of internal pores, the microcracks continue to sprout. Compared with the C0 M sample, the overall microstructure is more compact; when the chloride salt concentration of the corrosion solution increases to 3.5%, as shown in Fig. 9d, the concrete compactness is further improved, and the chloride salt content increases. As a result, a large number of NaCl crystals can fill up and refine the internal pores while reducing the connectivity of the pores in the latter stage of corrosion. In this case, the invasion of corrosive ions of  $\text{Mg}^{2+}$  and  $\text{SO}_4^{2-}$  can be inhibited slightly. Therefore, in this figure, only a few needle-like ettringites embedded in the concrete can be seen. Moreover, many cementing and some granular materials are also seen piled together. Through EDS analysis (Fig. 10b), the elemental composition of the non-cementing granular corrosion material includes Mg, O, Si, Na, Ca, and S. According to the interpretation of the morphology of the microscopic product by relevant literature [55], it can be judged that the corrosion product is probably M-S-H. The above FTIR analysis shows that the acidity and alkalinity inside the

concrete decrease at this time, and the undecomposed C-S-H decalcifies and the  $Mg^{2+}$  forms the non-cementing M-S-H, which accelerates the decrease of C-S-H content.

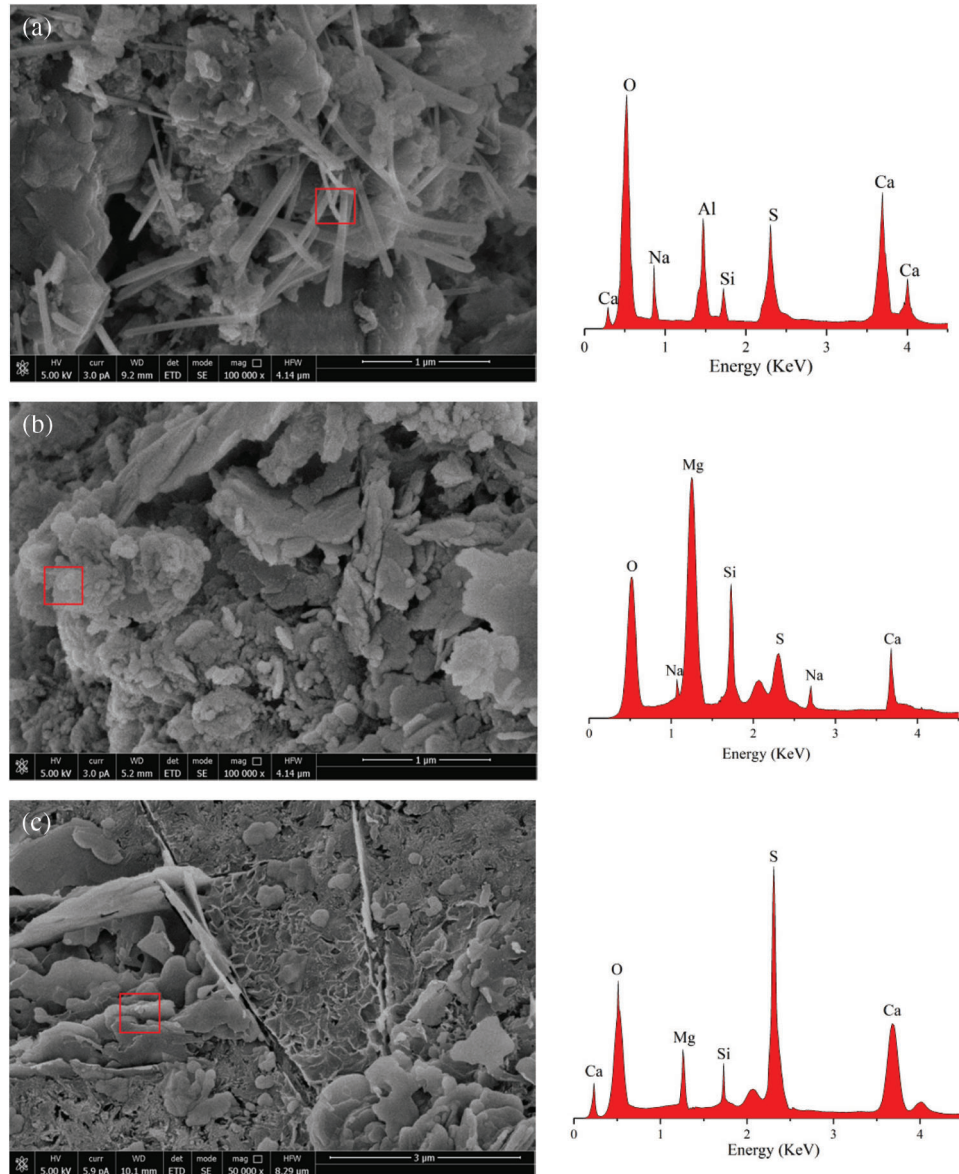


**Figure 10:** EDS spectra of samples with 120 cycle days: (a) ettringite in C0.5 M, (b) M-S-H in C3.5 M, (c) gypsum in C0.5 + M

When the concrete is corroded by the internal chloride salt and the external magnesium sulphate solution, as shown in Fig. 9e, a large crack appears in the microstructure, and the small cracks also keep extending around it; this damage is much more severe than those on the microstructures of C0.5 M and C3.5 M. Due to the decline of hydration products, spherical cement particles, and UFA particles are exposed. At the same time, it can be observed that many plate-shaped corrosion products are embedded in the pores of the concrete. The analysis of EDS (Fig. 10c) shows that the main element composition of this material is S, O, Ca, and Si; according to the main characteristics of this material [56,57], it can be

judged that the corrosion product may be gypsum. At this time, the gypsum crystals have grown abnormally and are intertwined. The test block is subjected to the expansion pressure of the corrosion product; during the dry-wet alternation, under the combined effects of the surface tension, which is formed by migration of capillary pores, the corrosion solution increases the cracks inside concrete. Fig. 9f shows the micromorphology when the chloride salt concentration in the concrete reaches 3.5%, and it can be seen that the number of pores and cracks inside the test blocks greatly increase at this time. Compared with the microstructure of the other five groups of samples, the internal structure loss of the Group C3.5 + M reaches the maximum; except for the large number of pores of different sizes on the surface, the corrosion products are distributed in a disorderly manner around the pores. Due to the high content of chloride salt in the concrete, the hydration products and cementing materials will be reduced at the initial stage of hydration, which will reduce the compactness of the concrete. Therefore, when the external corrosion solution corrodes the concrete, it is easy to damage the internal integrity of the test block. As the corrosion time increases, the formation of M-S-H increases the peeling amount of aggregate, and the pores are further enlarged, causing corrosion ions to enter the inside of the matrix again, and causing secondary damage. Therefore, the damage of the Group C3.5 + M is greater than that of the remaining groups.

#### 4 Conclusions

Through the dry-wet alternation test, the damage mechanism and the law of the mineral admixture concrete under simultaneous corrosion of internal chloride salt and external magnesium salt/sulphate/chloride salts, and under the corrosion of only external magnesium salt/sulphate/chloride salts are revealed respectively in this paper; the comparisons are made on the similarities and differences of the deterioration mechanisms of the mineral admixture concretes that are subjected to the two corrosion methods, and the influence of chloride salt concentration on the concrete properties is analysed through the tests on the physical and mechanical properties, ion content, and macroscopic and microscopic properties. The following conclusions are drawn according to the test results:

- (1) When the mineral admixture concrete is jointly eroded by highly concentrated internal chloride salt and external compound salts, the concrete damage is significantly higher than that caused only by external compound salts; the internal chloride salt with low concentration can inhibit the diffusion of external corrosive ions, so the damage of concrete therefrom would be smaller than that caused only by external  $\text{MgSO}_4$  solution, but the property is lower than that of the test blocks corroded by external  $\text{MgSO}_4 + \text{NaCl}$  solution.
- (2) For the concrete corroded by internal chloride salts and external sulphate/magnesium salts, the change in the corrosion time also impacted the test block properties. During 0–20 cycles of corrosion, the physical properties increase slowly, but slowed down the diffusion of sulphate ions. When the corrosion increases from 80 to 120 times, compared with the test blocks that are corroded by external chloride/magnesium/sulphate salts, it shows rapid decrease in physical properties and rapid increase of ion diffusion speed.
- (3) The chloride salt has a certain inhibitory effect on the diffusion of  $\text{SO}_4^{2-}$  and  $\text{Mg}^{2+}$ . When the mineral admixture concrete is only corroded by the external chloride/sulphate/magnesium salts, the increase of the external chloride salt concentration reduces the thaumasite, ettringite, and gypsum crystals inside the concrete and improves the durability of the test block.
- (4) The mineral admixture concrete is more severely damaged under the joint damage of  $\text{Mg}^{2+}$  and  $\text{SO}_4^{2-}$ . Macroscopically, it is manifested as the peeling of a large area of aggregate and the generation of a few cracks; microscopically, the corrosion products inside the concrete are mainly ettringite, gypsum, M-S-H,  $\text{Mg}(\text{OH})_2$ , and thaumasite. The joint damage of the corrosion

products worsens the internal connectivity of the test block and increases the number of pores and cracks.

**Funding Statement:** This research was funded by the Key Projects of Natural Science Research in Colleges and Universities of Anhui Province, Grant No. KJ2019A1043; Science and Technology Project of Jiangsu Provincial Department of Housing and Urban Rural Development, Grant No. 2019ZD001190.

**Conflicts of Interest:** The authors declare that they have no conflicts of interest to report regarding the present study.

## References

1. Nehdi, M. L., Suleiman, A. R., Soliman, A. M. (2014). Investigation of concrete exposed to dual sulfate attack. *Cement and Concrete Research*, 64, 42–53. DOI 10.1016/j.cemconres.2014.06.002.
2. Muthulingam, S., Rao, B. N. (2014). Non-uniform time-to-corrosion initiation in steel reinforced concrete under chloride environment. *Corrosion Science*, 82, 304–315. DOI 10.1016/j.corsci.2014.01.023.
3. Gu, Y. S., Martin, R. P., Metalssi, O. O., Fen, C. T., Dangla, P. (2019). Pore size analyses of cement paste exposed to external sulfate attack and delayed ettringite formation. *Cement and Concrete Research*, 123, 105766. DOI 10.1016/j.cemconres.2019.05.011.
4. Chen, E., Leung, C. K. Y. (2017). A coupled diffusion-mechanical model with boundary element method to predict concrete cover cracking due to steel corrosion. *Corrosion Science*, 126, 180–196. DOI 10.1016/j.corsci.2017.07.001.
5. Ann, K. Y., Song, H. W. (2007). Chloride threshold level for corrosion of steel in concrete. *Corrosion Science*, 49(11), 4113–4133. DOI 10.1016/j.corsci.2007.05.007.
6. Shanahan, N., Zayed, A. (2007). Cement composition and sulfate attack: Part I. *Cement and Concrete Research*, 37(4), 618–623. DOI 10.1016/j.cemconres.2006.12.004.
7. Dehwah, H. A. F. (2007). Effect of sulfate concentration and associated cation type on concrete deterioration and morphological changes in cement hydrates. *Construction and Building Materials*, 21(1), 29–39. DOI 10.1016/j.conbuildmat.2005.07.010.
8. Feng, P., Miao, C., Bullard, J. W. (2014). A model of phase stability, microstructure and properties during leaching of portland cement binders. *Cement and Concrete Composites*, 49, 9–19. DOI 10.1016/j.cemconcomp.2014.01.006.
9. Cheng, Y., Sun, W., Karen, S. (2013). Mechanism of expansion of mortars immersed in sodium sulfate solutions. *Cement and Concrete Research*, 43, 105–111. DOI 10.1016/j.cemconres.2012.10.001.
10. Weerdt, K. D., Justnes, H. (2015). The effect of sea water on the phase assemblage of hydrated cement paste. *Cement and Concrete Composites*, 55, 215–222. DOI 10.1016/j.cemconcomp.2014.09.006.
11. Zhao, H., Xiong, R., Guan, B. W. (2014). Fatigue damage property of cement concrete under magnesium sulfate corrosion condition. *Applied Mechanics and Materials*, 638–640, 1153–1157. DOI 10.4028/WWW.SCIENTIFIC.NET/AMM.638-640.1153.
12. Zhang, M. H., Li, H. (2011). Pore structure and chloride permeability of concrete containing nano-particles for pavement. *Construction and Building Materials*, 25(2), 608–616. DOI 10.1016/j.conbuildmat.2010.07.032.
13. Chang, H. L., Feng, P., Lyu, K., Liu, J. (2019). A novel method for assessing CSH chloride adsorption in cement pastes. *Construction and Building Materials*, 225, 324–331. DOI 10.1016/j.conbuildmat.2019.07.212.
14. Zhao, G. W., Shi, M., Fan, H. H., Cui, J. F., Xie, F. (2020). The influence of multiple combined chemical attack on cast-in-situ concrete: Deformation, mechanical development and mechanisms. *Construction and Building Materials*, 251, 118988. DOI 10.1016/j.conbuildmat.2020.118988.
15. Guan, B. W., Yang, T., Yu, D. M., Zhang, J. W., Ma, H. et al. (2016). Chloride ion erosion and life prediction of reinforced concrete under Dry and Wet cycling. *Materials Review*, 30(20), 152–157. DOI 10.11896/j.issn.1005-023X.2016.20.031.
16. Lee, S. J., Park, J. M. (2017). A study on the magnesium sulfate resistance of garnet fiber concrete. *Key Engineering Materials*, 730, 389–394. DOI 10.4028/WWW.SCIENTIFIC.NET/KEM.730.389.

17. Chen, Y. J., Gao, J. M., Tang, L. P., Li, X. H. (2016). Resistance of concrete against combined attack of chloride and sulfate under drying-wetting cycles. *Construction and Building Materials*, 106, 650–658. DOI 10.1016/j.conbuildmat.2015.12.151.
18. Stroh, J., Meng, B., Emmerling, F. (2016). Deterioration of hardened cement paste under combined sulphate-chloride attack investigated by synchrotron XRD. *Solid State Sciences*, 56, 29–44. DOI 10.1016/j.solidstatesciences.2016.04.002.
19. Maes, M., Belie, N. D. (2014). Resistance of concrete and mortar against combined attack of chloride and sodium sulphate. *Cement and Concrete Composites*, 53, 59–72. DOI 10.1016/j.cemconcomp.2014.06.013.
20. Qi, B., Gao, J. M., Chen, F., Shen, D. M. (2017). Evaluation of the damage process of recycled aggregate concrete under sulfate attack and wetting-drying cycles. *Construction and Building Materials*, 138, 254–262. DOI 10.1016/j.conbuildmat.2017.02.022.
21. Yuan, J., Liu, Y., Tan, Z., Zhang, B. (2016). Investigating the failure process of concrete under the coupled actions between sulfate attack and drying-wetting cycles by using X-ray CT. *Construction and Building Materials*, 108, 129–138. DOI 10.1016/j.conbuildmat.2016.01.040.
22. Bassuoni, M. T., Rahman, M. M. (2016). Response of concrete to accelerated physical salt attack exposure. *Cement and Concrete Research*, 79, 395–408. DOI 10.1016/j.cemconres.2015.02.006.
23. Santhanam, M., Cohen, M., Olek, J. (2006). Differentiating seawater and groundwater attack in portland cement mortars. *Cement and Concrete Research*, 36(12), 2132–2137. DOI 10.1016/j.cemconres.2006.09.011.
24. Scarfato, P., Maio, L. D., Fariello, M. L., Russoc, P., Incarnato, I. (2012). Preparation and evaluation of polymer/clay nanocomposite surface treatments for concrete durability enhancement. *Cement and Concrete Composites*, 34(3), 297–305. DOI 10.1016/j.cemconcomp.2011.11.006.
25. Huang, C. H., Lin, S. K., Chang, C. X., Chen, H. J. (2013). Mix proportions and mechanical properties of concrete containing very high-volume of class F fly ash. *Construction and Building Materials*, 46, 71–78. DOI 10.1016/j.conbuildmat.2013.04.016.
26. Chen, X., Sun, Z., Pang, J. (2021). A research on durability degradation of mineral admixture concrete. *Materials*, 14(7), 1752. DOI 10.3390/MA14071752.
27. Li, H., Xu, D. L., Feng, S. H., Shang, B. M. (2014). Microstructure and performance of fly ash micro-beads in cementitious material system. *Construction and Building Material*, 52, 422–427. DOI 10.1016/j.conbuildmat.2013.11.040.
28. Dhole, R., Thomas, M. D. A., Folliard, K. J., Drimalas, T. (2019). Chemical and physical sulfate attack on fly ash concrete mixtures. *Key Engineering Materials*, 116(4), 31–42. DOI 10.14359/51716678.
29. Alcamand, H. A., Borges, P. H. R., ASilva, F., Trindade, A. C. C. (2018). The effect of matrix composition and calcium content on the sulfate durability of metakaolin and metakaolin/slag alkali-activated mortars. *Ceramics International*, 44(5), 5037–5044. DOI 10.1016/j.ceramint.2017.12.102.
30. Goncalves, J. P., Toledo, R. D., Fairbairn, E. M. (2008). Evaluation of magnesium sulphate attack in mortar metakaolins system by thermal analysis. *Journal of Thermal Analysis and Calorimetry*, 94(2), 511–516. DOI 10.1007/S10973-007-8796-Y.
31. AliMardani, A., Gözde, S., Kambiz, R. (2014). Comparison of fly ash, silica finne and metakaolin from mechanical properties and durability performance of mortar mixtures view point. *Construction and Building Materials*, 70(15), 17–25. DOI 10.1016/j.conbuildmat.2014.07.089.
32. Li, J. P., Yao, M. B., Shao, W. (2016). Diffusion-reaction model of stochastically mixed sulfate in cast-*in-situ* piles. *Construction and Building Materials*, 115(15), 662–668. DOI 10.1016/j.conbuildmat.2016.04.075.
33. GB/T50082–2009 (2009). Standard for Test Method of Long-Term Performance and Durability of Ordinary Concrete. Beijing, China: Chinese Standard Institution Press.
34. GB/T50081–2002 (2002). Standard for Test Method of Mechanical Properties on Ordinary Concrete. Beijing, China: China Building Industry Press.
35. GB/T176–2008 (2008). Methods for Chemical Analysis of Cement. Beijing, China: Chinese Standard Institution Press.

36. Pan, C. L., Chu, H. Q., Jiang, L. H., Zhu, Z. Y., Wang, T. T. et al. (2019). Effect of cation types on chloride ion binding ability in chloride sulfate coexistence environment. *Concrete*, 4, 28–32. DOI 10.3969/j.issn.1002-3550.2019.04.007.
37. Cheng, S. K., Shui, Z. H., Sun, T., Gao, X., Guo, C. (2019). Effects of sulfate and magnesium ion on the chloride transportation behavior and binding capacity of portland cement mortar. *Construction and Building Materials*, 204, 265–275. DOI 10.1016/j.conbuildmat.2019.01.132.
38. Yu, H. F., Tan, Y. S., Yang, L. M. (2017). Microstructural evolution of concrete under the attack of chemical salt crystallization and bending stress. *Journal of Materials in Civil Engineering*, 29(7), 04017041. DOI 10.1061/(ASCE)MT.1943-5533.0001869.
39. Sujjavanich, S., Suwanvitaya, P., Chaysuwan, D., Heness, G. (2017). Synergistic effect of metakaolin and fly ash on properties of concrete. *Construction and Building Materials*, 155, 830–837. DOI 10.1016/j.conbuildmat.2017.08.072.
40. Zhang, Z. Y., Jin, X. G., Luo, W. (2019). Long-term behaviors of concrete under low-concentration sulfate attack subjected to natural variation of environmental climate conditions. *Cement and Concrete Research*, 116, 217–230. DOI 10.1016/j.cemconres.2018.11.017.
41. Jin, Z. Q., Sun, W., Zhang, Y. S., Jiang, J. Y., Lai, J. Z. (2007). Interaction between sulfate and chloride solution attack of concretes with and without fly ash. *Cement and Concrete Research*, 37(8), 1223–1232. DOI 10.1016/j.cemconres.2007.02.016.
42. Zhao, G. W., Li, J. P., Han, F., Shi, M., Fan, H. H. (2019). Sulfate-induced degradation of cast-in-situ concrete influenced by magnesium. *Construction and Building Materials*, 199, 194–206. DOI 10.1016/j.conbuildmat.2018.12.022.
43. Cheng, S. K., Shui, Z. H., Sun, T., Gao, X., Guo, C. (2019). Effects of sulfate and magnesium ion on the chloride transportation behavior and binding capacity of portland cement mortar. *Construction and Building Materials*, 204, 265–275. DOI 10.1016/j.conbuildmat.2019.01.132.
44. Weerdt, K. D., Lothenbach, B., Geiker, M. R. (2019). Comparing chloride ingress from seawater and NaCl solution in portland cement mortar. *Cement and Concrete Research*, 115, 80–89. DOI 10.1016/j.cemconres.2018.09.014.
45. Shanahan, N., Sedaghat, A., Zayed, A. (2016). Effect of cement mineralogy on the effectiveness of chloride-based accelerator. *Cement and Concrete Composites*, 73, 226–234. DOI 10.1016/j.cemconcomp.2016.07.015.
46. Thoma, J. J., Allen, A. J., Jennings, H. M. (2009). Hydration kinetics and microstructure development of normal and CaCl<sub>2</sub>-accelerated tricalcium silicate pastes. *The Journal of Physical Chemistry*, 113(46), 19836–19844. DOI 10.1021/JP907078U.
47. Wang, J. B., Niu, D. T., Hui, H., Wang, B. (2019). Study on durability degradation of shotcrete lining eroded by compound salt. *Journal of Civil Engineering*, 52(9), 79–90. DOI 10.15951/j.tmgcxb.2019.09.006.
48. Ismail, I., Bernal, S. A., Provis, J. L., Hamdan, S., Deventer, J. S. J. V. (2013). Microstructural changes in alkali activated fly ash/slag geopolymers with sulfate exposure. *Materials and Structures*, 46(3), 361–373. DOI 10.1617/S11527-012-9906-2.
49. Deng, D. H., Xiao, J., Yuan, Q., Zhang, W. N., Liu, Y. X. (2005). On thaumasite incementitious materials. *Journal of Building Materials*, 8(4), 400–409.
50. Bernard, E., Lothenbach, B., Rentsch, D., Pochard, I., Dauzères, A. (2017). Formation of magnesium silicate hydrates (M-S-H). *Physics & Chemistry of the Earth Parts A/B/C*, 99, 142–157. DOI 10.1016/j.pce.2017.02.005.
51. Song, K. I., Yang, K. H., Lee, B. Y., Song, K. H. (2014). Carbonation characteristics of alkaliactivated blast-furnace slag mortar. *Advances in Materials Science and Engineering*, 2014, 1–11. DOI 10.4334/JKCI.2012.24.3.315.
52. Nied, D., Enemark-Rasmussen, K., Lhopital, E., Skibsted, J. (2016). Properties of magnesium silicate hydrates (M-S-H). *Cement and Concrete Research*, 79, 323–332. DOI 10.1016/j.cemconres.2015.10.003.
53. Sarkar, S., Mahadevan, S., Meeussen, J. C. L., van der Sloot, H., Kosson, D. S. (2010). Numerical simulation of cementitious materials degradation under external sulfate attack. *Cement and Concrete Composites*, 32(3), 241–252. DOI 10.1016/j.cemconcomp.2009.12.005.

54. Nehdi, M. L., Suleiman, A. R., Soliman, A. M. (2014). Investigation of concrete exposed to dual sulfate attack. *Cement and Concrete Research*, 64, 42–53. DOI 10.1016/j.cemconres.2014.06.002.
55. Li, Z. H., Zhang, T. S., Hu, J., Tang, Y., Niu, Y. F. et al. (2014). Characterization of reaction products and reaction process of MgO-SiO<sub>2</sub>-H<sub>2</sub>O system at room temperature. *Construction and Building Materials*, 61, 252–259. DOI 10.1016/j.conbuildmat.2014.03.004.
56. Tan, Y., Yu, H., Ma, H., Zhang, Y., Wu, C. (2017). Study on the micro-crack evolution of concrete subjected to stress corrosion and magnesium sulfate. *Construction and Building Materials*, 141, 453–460. DOI 10.1016/j.conbuildmat.2017.02.127.
57. Collepardi, M. (2003). A state-of-the-art review on delayed ettringite attack on concrete. *Cement and Concrete Composites*, 25(4–5), 401–407. DOI 10.1016/S0958-9465(02)00080-X.